Effects of hexagonal warping on surface transport in topological insulators

C. M. Wang* and F. J. Yu

School of Physics and Electrical Engineering, Anyang Normal University, Anyang 455000, China

(Received 7 April 2011; revised manuscript received 30 June 2011; published 28 October 2011)

We investigate the charge conductivity and current-induced spin polarization of the surface state of a three-dimensional topological insulator by including the hexagonal-warping effect of the Fermi surface in both the classical and quantum diffusion regimes. We present general expressions of conductivity and spin polarization, which are reduced to simple forms for the usual scattering potential. Due to the hexagonal warping, the conductivity and spin polarization show an additional quadratic carrier-density dependence both for the Boltzmann contribution and the quantum correction. In the presence of the warping term, the surface states still reveal weak antilocalization. Moreover, the dielectric function in the random phase approximation is also explored, and we find that it may be momentum-angle-dependent.

DOI: 10.1103/PhysRevB.84.155440 PACS number(s): 73.25.+i, 72.10.−d, 73.20.At

I. INTRODUCTION

Topological insulators (TIs) have attracted a great deal of research both experimentally and theoretically in the past few years[1–3] due to their potential applications in topological quantum computation[4] and spintronics.[5] A TI has a full energy gap in bulk while it has gapless surface states stable against weak disorder and weak interaction unless the time-reversal symmetry is broken.[6,7] In particular and in vivid contrast with graphene,[8] the number of its Dirac points is odd according to a no-go theorem.[6] Hence, many theoretical studies focus on a class of TI in which the surface states only consist of one Dirac cone.

Experimentally, this surface state has been well confirmed by angle-resolved photoemission spectroscopy (ARPES).[9–11] However, the transport observation of the surface state in the classical diffusion regime encounters an obstacle due to the large bulk-conduction background. Recently, Checkelsky *et al*. claimed to have isolated the surface-band contribution in Bi_2Se_3 by electrostatic gate control of the chemical potential.[12] Nevertheless, this work is questionable given that the chemical potential is still in the bulk conduction band.[13] Culcer *et al*. theoretically investigated the two-dimensional surface charge transport and obtained results analogous to those of graphene.[13] Recently, Kim *et al*. showed that the surface of thin Bi_2Se_3 was strongly electrostatically coupled.[14] They observed the surface transport by using a gate electrode to remove bulk charge carriers completely and effectively demonstrated the theoretical prediction.[13] It is very likely that this experiment has overcome the abovementioned obstacle. Also, the anomalous Hall conductivity of the surface of TIs was calculated using the quantum Liouville equation.[15] The conductivity due to electron-phonon scattering was investigated for the surface state of a strong TI.[16] Moreover, transverse magnetic heat transport was explored on the topological surface.[17]

On the other hand, recently the quantum corrections to charge conductivity in topological surface states were also extensively studied.[12,18–22] The surface states in the quantum diffusion regime ($l_\phi \gg l$) reveal a positive correction to the conductivity correction, i.e., weak antilocalization, which is related to the π Berry phase.[21] Here, l and l_ϕ are the elastic-scattering length and the phase-coherence length, respectively. In contrast with graphene in which the weak antilocalization is suppressed by intervalley scattering,[23] the surface state of a TI forbids this scattering process due to a single Dirac cone, and many observations have confirmed this enhancement to the electronic conductivity.[12,18–20] Lu *et al*. found that the surface state of a TI shows a competing effect of weak localization and weak antilocalization in quantum transport due to magnetic doping.[21]

We have noted that in most of these theoretical studies, only the $\boldsymbol{k}$-linear term in the spin-orbit interaction is present in the effective Hamiltonian. However, in some TIs, for example Bi_2Te_3, ARPES[11] and scanning-tunneling-microscopy[24] measurements revealed that the shape of the Fermi surface changes from a circle to a hexagon and then to a snowflakelike shape with increasing Fermi energy. With the help of a hexagonal-warping term, this kind of band structure was explained by Fu.[25] Note that the states near the Fermi surface are responsible for the transport properties at low temperatures. Hence, it is expected that the warping effect will naturally play a significant role on surface transport when the Fermi energy is high enough. So far, only one theoretical work in the literature has involved the warping effect on the weak antilocalization.[22] Furthermore, they simply replaced the warping term by its angle-average term; hence, the anisotropy of the energy spectrum due to warping is neglected completely. Then they acquired the same form of correction as the usual two-dimensional electron gas with spin-orbital interaction. Consequently, it is highly desirable to carefully study the warping effect on the classical contribution and quantum correction to the surface transport.

In this paper, we study the hexagonal-warping effect on the charge conductivity and current-induced spin polarization (CISP) of the surface state of a three-dimensional TI. Considering nonmagnetic and magnetic elastic carrier-impurity scattering, we discuss this problem in both the classical and quantum diffusive regimes. We also investigate the warping effect on the dielectric function in the random phase approximation (RPA). The structure of the paper is as follows. In Sec. II, the effective Hamiltonian of the surface state is given. By using a kinetic-equation approach, the conductivity and CISP in the classical transport regime in the presence of nonmagnetic and magnetic scattering are calculated in Secs. III

and IV. In Sec. V, we discuss the quantum correction to the conductivity and CISP. A brief summary is given in Sec. VI.

II. THE SYSTEM AND HAMILTONIAN

By assuming particle-hole symmetry, the effective Hamiltonian of the surface state of a TI, including the hexagonal-warping effect, has the following form:

$$\hat{H}_0 = v_{\rm F}(k_x\hat{\sigma}_y - k_y\hat{\sigma}_x) + \frac{\lambda}{2}(k_+^3 + k_-^3)\hat{\sigma}_z. \tag{1}$$

Here, $v_{\rm F}$ and λ are the Fermi velocity and the hexagonal-warping constant, respectively; $\hat{\sigma}_i$ $(i = x,y,z)$ are the Pauli matrices; and $k_\pm = k_x \pm ik_y$. The quadratic term $k^2/(2m)$ is in principle also present in the Hamiltonian with m denoting the effective mass of the particle, but it is smaller than the $\boldsymbol{k}$-linear and cubic terms due to the relation $2mv_{\rm F} \gg \sqrt{v_{\rm F}/\lambda}$ in Bi_2Te_3. Consequently, in the regime of density 10^{13} cm^{-2} $< N < 10^{14}$ cm^{-2}, both the linear and cubic terms contribute significantly to the transport quantities, and the quadratic term can be safely neglected. Near the regime $\boldsymbol{k} = 0$, the cubic correction is also negligible. However, at high densities, the cubic term makes the energy spectrum of the surface state angle dependent, and the Fermi surface becomes snowflakelike.

The eigenenergies of the considered system of Eq. (1) are $\varepsilon_{\boldsymbol{k}\mu} = (-1)^\mu\epsilon_{\boldsymbol{k}}$, where

$$\epsilon_{\boldsymbol{k}} = \sqrt{(v_{\rm F}k)^2 + (\lambda k^3\cos 3\theta_{\boldsymbol{k}})^2} \tag{2}$$

with an azimuthal angle of $\boldsymbol{k}$, $\theta_{\boldsymbol{k}} = \tan^{-1}(k_y/k_x)$, and an index $\mu = 1,2$. By introducing the angle

$$\beta_{\boldsymbol{k}} = \tan^{-1}\sqrt{\frac{\epsilon_{\boldsymbol{k}} - \lambda k^3\cos 3\theta_{\boldsymbol{k}}}{\epsilon_{\boldsymbol{k}} + \lambda k^3\cos 3\theta_{\boldsymbol{k}}}}, \tag{3}$$

the corresponding eigenstates $\varphi_{\boldsymbol{k}\mu}$ are written as

$$\varphi_{\boldsymbol{k}1} = \begin{pmatrix} \sin\beta_{\boldsymbol{k}} \\ -i\cos\beta_{\boldsymbol{k}}e^{i\theta_{\boldsymbol{k}}} \end{pmatrix}, \tag{4}$$

$$\varphi_{\boldsymbol{k}2} = \begin{pmatrix} \cos\beta_{\boldsymbol{k}} \\ i\sin\beta_{\boldsymbol{k}}e^{i\theta_{\boldsymbol{k}}} \end{pmatrix}. \tag{5}$$

It should be noted that the above Hamiltonian [Eq. (1)] can be diagonalized to $H_0 = U_{\boldsymbol{k}}^\dagger\hat{H}_0U_{\boldsymbol{k}} = {\rm diag}(\varepsilon_{\boldsymbol{k}1},\varepsilon_{\boldsymbol{k}2})$ with the help of the local unitary transformation $U_{\boldsymbol{k}} = (\varphi_{\boldsymbol{k}1},\varphi_{\boldsymbol{k}2})$. This transformation projects the system from the spin basis to the eigenbasis of $\hat{H}_0$.

III. CLASSICAL TRANSPORT IN THE PRESENCE OF NONMAGNETIC SCATTERING

A. Kinetic equations

In order to study the transport property of the surface state in the classical diffusive regime, we limit our system to a spatially homogeneous one. First, we consider the nonmagnetic carrier-impurity elastic scattering and focus on the charge transport at the Fermi level inside the bulk gap of the TI. The kinetic equation for the single-particle distribution function in the eigenbasis of $\hat{H}_0$, $\rho(\boldsymbol{k})$, is constructed using the nonequilibrium Green's function and is given by[26]

$$\left(\frac{\partial}{\partial T} - e\boldsymbol{E}\cdot\nabla_{\boldsymbol{k}}\right)\rho + e\boldsymbol{E}\cdot[\rho, U_{\boldsymbol{k}}^\dagger\nabla_{\boldsymbol{k}}U_{\boldsymbol{k}}] + i[\hat{H}_0,\rho] = -I_{\rm sc}. \tag{6}$$

Here $\boldsymbol{E}$ is the electric field. It should be noted that here $\rho(\boldsymbol{k})$ is a 2×2 matrix. In the lowest order of the gradient expansion, the scattering integral $I_{\rm sc}$ can be written as $I_{\rm sc} = \int_{-\infty}^{T} dt'(\Sigma^r G^< + \Sigma^< G^a - G^r\Sigma^< - G^<\Sigma^a)(T,t')(t',T)$ with $\Sigma^{<,r,a}$ being the lesser, retarded, and advanced self-energies in the self-consistent Born approximation, respectively. We consider that the scattering by impurities at random positions $\{\boldsymbol{R}_\alpha\}$ has the form $\widetilde{V}(\boldsymbol{r}) = \sum_{\{\boldsymbol{R}_\alpha\}} V(\boldsymbol{r} - \boldsymbol{R}_\alpha)$. Therefore, after impurity averaging,[26] the self-energies in the eigenbasis of $\hat{H}_0$ read $\Sigma^{<,r,a}(\boldsymbol{k}) = n_i\sum_{\boldsymbol{q}}|V(\boldsymbol{k}-\boldsymbol{q})|^2U_{\boldsymbol{k}}^\dagger U_{\boldsymbol{q}}G^{<,r,a}(\boldsymbol{q})U_{\boldsymbol{q}}^\dagger U_{\boldsymbol{k}}$ with n_i denoting the impurity density and $V(\boldsymbol{q})$ being the Fourier transform of $V(\boldsymbol{r})$.

Furthermore, we take the generalized Kadanoff-Baym ansatz[26] and ignore the collisional broadening to simplify the scattering integral. Throughout this paper, we focus on the situation in which the Fermi energy $\varepsilon_{\rm F}$ is positive, i.e., the Fermi energy is in the conduction band of the surface state, and assume the electric field is along the x direction. For the lowest order of the impurity density n_i and stationary electric field $\boldsymbol{E} = E\hat{x}$, the solution of the equation can be written as $\rho(\boldsymbol{k}) = \rho^{(0)}(\boldsymbol{k}) + \rho^{(1)}(\boldsymbol{k}) + \rho^{(2)}(\boldsymbol{k})$. Here, $\rho^{(0)}(\boldsymbol{k}) = {\rm diag}[n_{\rm F}(\varepsilon_{\boldsymbol{k}1}),n_{\rm F}(\varepsilon_{\boldsymbol{k}2})]$ [$n_{\rm F}(x)$ is the Fermi-Dirac function] is the equilibrium distribution function. $\rho^{(1)}(\boldsymbol{k})$ and $\rho^{(2)}(\boldsymbol{k})$ are two distribution functions proportional to the electric field. $\rho^{(1)}(\boldsymbol{k})$ is the impurity-independent distribution function, and only the off-diagonal elements $\rho_{12}^{(1)}(\boldsymbol{k}) = \rho_{21}^{(1)*}(\boldsymbol{k}) = \rho_r^{(1)}(\boldsymbol{k}) + i\rho_i^{(1)}(\boldsymbol{k})$ are nonzero with

$$\rho_r^{(1)}(\boldsymbol{k}) = \frac{eE}{4k\epsilon_{\boldsymbol{k}}}\sin 2\beta_{\boldsymbol{k}}\sin\theta_{\boldsymbol{k}}[n_{\rm F}(\varepsilon_{\boldsymbol{k}1}) - n_{\rm F}(\varepsilon_{\boldsymbol{k}2})], \tag{7}$$

$$\rho_i^{(1)}(\boldsymbol{k}) = \frac{eE}{16k\epsilon_{\boldsymbol{k}}}\frac{\sin 4\beta_{\boldsymbol{k}}(\cos 4\theta_{\boldsymbol{k}} - 5\cos 2\theta_{\boldsymbol{k}})}{\cos 3\theta_{\boldsymbol{k}}} \times[n_{\rm F}(\varepsilon_{\boldsymbol{k}1}) - n_{\rm F}(\varepsilon_{\boldsymbol{k}2})]. \tag{8}$$

$\rho^{(2)}(\boldsymbol{k})$ relies on the carrier-impurity scattering, and its elements are determined by the following set of equations:

$$eE\frac{\partial}{\partial k_x}n_{\rm F}(\varepsilon_{\boldsymbol{k}2}) = 2\pi n_i\sum_{\boldsymbol{q}}|V(\boldsymbol{k}-\boldsymbol{q})|^2a_1(\boldsymbol{k},\boldsymbol{q}) \times\left[\rho_{22}^{(2)}(\boldsymbol{k}) - \rho_{22}^{(2)}(\boldsymbol{q})\right]\delta(\varepsilon_{\boldsymbol{k}2} - \varepsilon_{\boldsymbol{q}2}), \tag{9}$$

$$2\epsilon_{\boldsymbol{k}}\rho_i^{(2)}(\boldsymbol{k}) = \pi n_i\sum_{\boldsymbol{q}}|V(\boldsymbol{k}-\boldsymbol{q})|^2a_2(\boldsymbol{k},\boldsymbol{q}) \times\left[\rho_{22}^{(2)}(\boldsymbol{k}) - \rho_{22}^{(2)}(\boldsymbol{q})\right]\delta(\varepsilon_{\boldsymbol{k}2} - \varepsilon_{\boldsymbol{q}2}), \tag{10}$$

$$-2\epsilon_{\boldsymbol{k}}\rho_r^{(2)}(\boldsymbol{k}) = \pi n_i\sum_{\boldsymbol{q}}|V(\boldsymbol{k}-\boldsymbol{q})|^2a_3(\boldsymbol{k},\boldsymbol{q}) \times\left[\rho_{22}^{(2)}(\boldsymbol{k}) - \rho_{22}^{(2)}(\boldsymbol{q})\right]\delta(\varepsilon_{\boldsymbol{k}2} - \varepsilon_{\boldsymbol{q}2}). \tag{11}$$

$\rho_r^{(2)}(\boldsymbol{k})$ and $\rho_i^{(2)}(\boldsymbol{k})$ are the real and imaginary parts of $\rho_{12}^{(2)}(\boldsymbol{k})$, respectively. In these equations,

$$a_1(\boldsymbol{k},\boldsymbol{q}) = \tfrac{1}{2}[\sin 2\beta_{\boldsymbol{k}} \sin 2\beta_{\boldsymbol{q}} \cos(\theta_{\boldsymbol{k}} - \theta_{\boldsymbol{q}}) + \cos 2\beta_{\boldsymbol{k}} \cos 2\beta_{\boldsymbol{q}} + 1], \tag{12}$$

$$a_2(\boldsymbol{k},\boldsymbol{q}) = \tfrac{1}{2}[\cos 2\beta_{\boldsymbol{k}} \sin 2\beta_{\boldsymbol{q}} \cos(\theta_{\boldsymbol{k}} - \theta_{\boldsymbol{q}}) - \sin 2\beta_{\boldsymbol{k}} \cos 2\beta_{\boldsymbol{q}}], \tag{13}$$

$$a_3(\boldsymbol{k},\boldsymbol{q}) = -\tfrac{1}{2} \sin 2\beta_{\boldsymbol{q}} \sin(\theta_{\boldsymbol{k}} - \theta_{\boldsymbol{q}}). \tag{14}$$

Note the requirement that $\varepsilon_{\mathrm{F}} > 0$ despite the assumption that the Fermi energy is in the gap of the bulk system; hence, the diagonal element $\rho_{11}^{(2)}(\boldsymbol{k})$ makes no contribution to the transport equations. We find that when $\theta_{\boldsymbol{k}} - \theta_{\boldsymbol{q}} = \pi$, $a_1(\boldsymbol{k},\boldsymbol{q}) = \frac{1}{2}[\cos(2\beta_{\boldsymbol{k}} - 2\beta_{\boldsymbol{q}}) + 1] = 0$. This reveals the absence of backscattering, a characteristic of TIs.

B. Conductivity and CISP

In the eigenbasis of $\hat{H}_0$, the average velocity $\boldsymbol{v} = \frac{1}{N}\sum_{\boldsymbol{k}} \mathrm{Tr}[\rho(\boldsymbol{k}) U_{\boldsymbol{k}}^{\dagger} \hat{\boldsymbol{v}} U_{\boldsymbol{k}}]$. Here, two components of the velocity operator in the spin basis are written as

$$\hat{v}_x = \begin{pmatrix} 3\lambda k^2 \cos 2\theta_{\boldsymbol{k}} & -i v_{\mathrm{F}} \\ i v_{\mathrm{F}} & -3\lambda k^2 \cos 2\theta_{\boldsymbol{k}} \end{pmatrix}, \tag{15}$$

$$\hat{v}_y = \begin{pmatrix} -3\lambda k^2 \sin 2\theta_{\boldsymbol{k}} & -v_{\mathrm{F}} \\ -v_{\mathrm{F}} & 3\lambda k^2 \sin 2\theta_{\boldsymbol{k}} \end{pmatrix}. \tag{16}$$

It is seen that the diagonal elements of the velocity operator are also nonzero when we include the warping term. Therefore, the longitudinal and transverse conductivities $\sigma_{xx} = -Nev_x/E$ and $\sigma_{xy} = -Nev_y/E$ can be expressed as

$$\sigma_{xx} = -\frac{e}{E}\sum_{\boldsymbol{k}} [(v_{\mathrm{F}} \sin 2\beta_{\boldsymbol{k}} \cos\theta_{\boldsymbol{k}} + 3\lambda k^2 \cos 2\beta_{\boldsymbol{k}} \cos 2\theta_{\boldsymbol{k}}) \times \rho_{22}(\boldsymbol{k}) - 2(v_{\mathrm{F}} \cos 2\beta_{\boldsymbol{k}} \cos\theta_{\boldsymbol{k}} - 3\lambda k^2 \sin 2\beta_{\boldsymbol{k}} \cos 2\theta_{\boldsymbol{k}}) \times \rho_r(\boldsymbol{k}) + 2v_{\mathrm{F}} \sin\theta_{\boldsymbol{k}} \rho_i(\boldsymbol{k})], \tag{17}$$

$$\sigma_{xy} = -\frac{e}{E}\sum_{\boldsymbol{k}} [(v_{\mathrm{F}} \sin 2\beta_{\boldsymbol{k}} \sin\theta_{\boldsymbol{k}} - 3\lambda k^2 \cos 2\beta_{\boldsymbol{k}} \sin 2\theta_{\boldsymbol{k}}) \times \rho_{22}(\boldsymbol{k}) - 2(v_{\mathrm{F}} \cos 2\beta_{\boldsymbol{k}} \sin\theta_{\boldsymbol{k}} + 3\lambda k^2 \sin 2\beta_{\boldsymbol{k}} \sin 2\theta_{\boldsymbol{k}}) \times \rho_r(\boldsymbol{k}) - 2v_{\mathrm{F}} \cos\theta_{\boldsymbol{k}} \rho_i(\boldsymbol{k})]. \tag{18}$$

The hexagonal-warping term results in the complex forms of the charge conductivities. In the surface state of a TI, the carrier spin is directly coupled to the momentum in contrast with graphene. Hence, in this system an external in-plane electric field can lead to a uniform spin polarization[13] as in spin-orbit-coupled systems.[27–30] This is the so-called CISP. The three components of the CISP $\boldsymbol{S} = \sum_{\boldsymbol{k}} \mathrm{Tr}[\rho(\boldsymbol{k}) U_{\boldsymbol{k}}^{\dagger} \frac{1}{2}\hat{\boldsymbol{\sigma}} U_{\boldsymbol{k}}]$ are given by

$$S_x = \frac{1}{2}\sum_{\boldsymbol{k}} [-\sin 2\beta_{\boldsymbol{k}} \sin\theta_{\boldsymbol{k}} \rho_{22}(\boldsymbol{k}) + 2\cos 2\beta_{\boldsymbol{k}} \sin\theta_{\boldsymbol{k}} \rho_r(\boldsymbol{k}) + 2\cos\theta_{\boldsymbol{k}} \rho_i(\boldsymbol{k})], \tag{19}$$

$$S_y = \frac{1}{2}\sum_{\boldsymbol{k}} [\sin 2\beta_{\boldsymbol{k}} \cos\theta_{\boldsymbol{k}} \rho_{22}(\boldsymbol{k}) - 2\cos 2\beta_{\boldsymbol{k}} \cos\theta_{\boldsymbol{k}} \rho_r(\boldsymbol{k}) + 2\sin\theta_{\boldsymbol{k}} \rho_i(\boldsymbol{k})], \tag{20}$$

$$S_z = \frac{1}{2}\sum_{\boldsymbol{k}} [\cos 2\beta_{\boldsymbol{k}} \rho_{22}(\boldsymbol{k}) + 2\sin 2\beta_{\boldsymbol{k}} \rho_r(\boldsymbol{k})]. \tag{21}$$

It is noticeable that the general Eqs. (17)–(21) are applicable to any scattering potential.

According to the Eqs. (7) and (8), it is seen that $\rho_r^{(1)}(k_x,k_y) = (-1)^n \rho_r^{(1)}[(-1)^m k_x,(-1)^n k_y]$ and $\rho_i^{(1)}(k_x,k_y) = \rho_i^{(1)}[(-1)^m k_x,(-1)^n k_y]$ with $m,n = 1,2$. We find that the impurity-independent distribution makes no contribution to the charge conductivity or the CISP. Furthermore, for normal nonmagnetic elastic scattering, the potential satisfies the following relation:[31]

$$V(q,\theta_{\boldsymbol{q}}) = V(q,\theta_{\boldsymbol{q}} - \pi) = V(q,\theta_{\boldsymbol{q}} + \pi). \tag{22}$$

In connection with the kinetic Eqs. (9)–(11), one can directly arrive at the symmetrical relation: $\rho_{22}^{(2)}(k_x,k_y) = (-1)^m \rho_{22}^{(2)}[(-1)^m k_x,(-1)^n k_y]$, $\rho_r^{(2)}(k_x,k_y) = (-1)^n \rho_r^{(2)}[(-1)^m k_x,(-1)^n k_y]$, and $\rho_i^{(2)}(k_x,k_y) = \rho_i^{(2)}[(-1)^m k_x,(-1)^n k_y]$. Therefore, it is clear that $\sigma_{xy} = 0$ and $S_x = S_z = 0$, and the off-diagonal elements of the distribution function have no effect on the charge conductivity or spin polarization. Accordingly, the longitudinal conductivity σ_{xx} and the y component of the spin polarization can be rewritten as

$$\sigma_{xx} = -\frac{e}{E}\sum_{\boldsymbol{k}} (v_{\mathrm{F}} \sin 2\beta_{\boldsymbol{k}} \cos\theta_{\boldsymbol{k}} + 3\lambda k^2 \cos 2\beta_{\boldsymbol{k}} \cos 2\theta_{\boldsymbol{k}}) \rho_{22}^{(2)}(\boldsymbol{k}), \tag{23}$$

$$S_y = \frac{1}{2}\sum_{\boldsymbol{k}} \sin 2\beta_{\boldsymbol{k}} \cos\theta_{\boldsymbol{k}} \rho_{22}^{(2)}(\boldsymbol{k}). \tag{24}$$

For vanishing λ, the spin polarization linearly depends on the longitudinal conductivity:

$$\frac{\sigma_{xx}}{S_y} = -2\frac{e v_{\mathrm{F}}}{E}. \tag{25}$$

This relation is valid for any nonmagnetic elastic scattering. The CISP can be observed using the Kerr rotation experiment.[32] Since CISP is characteristic of the surface state and there is no spin polarization in bulk TIs, this relation may provide a simple transport method to isolate the surface-conductivity contribution in Bi_2Se_3. One would first measure the surface spin polarization, and then the surface-conductivity contribution can be obtained from this relation. The remaining contribution of the conductivity can be considered to originate from the bulk band. However, this method is not applicable for Bi_2Te_3 due to its large warping effect.

The physical reason why only the y component of the CISP exists is as follows. The CISP arises because an electric field results in an average momentum $\langle \boldsymbol{k} \rangle = -e\boldsymbol{E}\tau_{\rm tr}$ with $\tau_{\rm tr}$ being the transport lifetime. This implies from Hamiltonian (1) that there is an average spin-orbit field. This effective magnetic field leads to this spin polarization. When the electric field is applied along the x direction, only the y and z components of the average effective magnetic field are nonzero. Furthermore, the z component is a higher-order term of the electric field and transport lifetime. Hence, in the limit of a weak electric field and weak scattering, only the y component of the spin polarization is nonzero. We emphasize that this argument is very general and valid for all scattering, including inelastic phonon scattering.

C. δ-form short-range potential

We first limit ourselves to δ-form short-range nonmagnetic scattering $\widetilde{V}(\boldsymbol{r}) = \sum_{\{\boldsymbol{R}_\alpha\}} u\delta(\boldsymbol{r} - \boldsymbol{R}_\alpha)$. This scattering arises from the surface roughness. For this potential, Eq. (22) is satisfied explicitly. Hence, only the longitudinal conductivity and y component of the CISP exist. Expanded to the second order of λ, the diagonal element of the matrix distribution function $\rho_{22}^{(2)}(\boldsymbol{k})$ can be obtained analytically. At zero temperature, it takes the form

$$\rho_{22}^{(2)}(\boldsymbol{k}) = -\frac{2eE}{n_i u^2}\Bigg[\frac{2v_{\rm F}^3}{\varepsilon_{\rm F}}\cos\theta_{\boldsymbol{k}} + \lambda^2\frac{\varepsilon_{\rm F}^3}{4v_{\rm F}^3}(18\cos\theta_{\boldsymbol{k}} + 5\cos 5\theta_{\boldsymbol{k}} - \cos 7\theta_{\boldsymbol{k}})\Bigg]\delta(\varepsilon_{\boldsymbol{k}2} - \varepsilon_{\rm F}). \tag{26}$$

Substituting the resultant distribution function into Eqs. (23) and (24), the longitudinal conductivity σ_{xx} and spin polarization S_y read

$$\sigma_{xx} = \frac{e^2}{\pi n_i u^2}\left[v_{\rm F}^2 + 2\left(\frac{\varepsilon_{\rm F}}{v_{\rm F}}\right)^4\lambda^2\right] = \frac{e^2}{\pi n_i u^2}\left(v_{\rm F}^2 + 32\pi^2\lambda^2N^2\right), \tag{27}$$

$$S_y = -\frac{eE}{4\pi n_i u^2}\left(2v_{\rm F} + \frac{\varepsilon_{\rm F}^4}{v_{\rm F}^5}\lambda^2\right) = -\frac{eE}{2\pi v_{\rm F} n_i u^2}\left(v_{\rm F}^2 + 8\pi^2\lambda^2N^2\right). \tag{28}$$

The hexagonal-warping parameter λ leads to quadratic corrections of the carrier density in the longitudinal conductivity σ_{xx} and CISP S_y. At the same time, the linear relation between σ_{xx} and S_y is broken. We emphasize here that the Hamiltonian for $\lambda = 0$ used in this paper is different from that of Ref. 13 for $D = 0$, replacing $\hat{\sigma}_y \to \hat{\sigma}_x$ and $\hat{\sigma}_x \to -\hat{\sigma}_y$. Hence, for vanishing λ, the above results are in agreement with previous ones.[13] It is noticeable that the effective Hamiltonian (1) is obtained for low-energy systems, and the above two equations are valid in the density regime $10^{13}\ {\rm cm}^{-2} < N < 10^{14}\ {\rm cm}^{-2}$ for Bi_2Te_3. This is the precondition of this entire work. Hence, all the equations are limited by this concealed condition.

D. Screened Coulomb potential

We now consider the screened Coulomb potential for which the screening function is in the RPA: $\epsilon_{\rm RPA}(\boldsymbol{q},\omega) = 1 - v_c(q)\Pi(\boldsymbol{q};\omega)$ with $v_c(q) = e^2/(2\epsilon_0\kappa q)$ being the two-dimensional Coulomb interaction. The charged-impurity scattering on the surface of a TI can be modeled by this potential well. The corresponding polarizability function takes the form

$$\Pi(\boldsymbol{q};\omega) = \sum_{\boldsymbol{k},\mu,\mu'}(\varphi^\dagger_{\boldsymbol{k}+\boldsymbol{q}\mu}\varphi_{\boldsymbol{k}\mu'})(\varphi^\dagger_{\boldsymbol{k}\mu'}\varphi_{\boldsymbol{k}+\boldsymbol{q}\mu}) \times\frac{n_{\rm F}(\varepsilon_{\boldsymbol{k}\mu'}) - n_{\rm F}(\varepsilon_{\boldsymbol{k}+\boldsymbol{q}\mu})}{\omega + \varepsilon_{\boldsymbol{k}\mu'} - \varepsilon_{\boldsymbol{k}+\boldsymbol{q}\mu} + i\eta}. \tag{29}$$

The warping term complicates the calculation of the polarizability function, and we cannot determine an analytical result even for a static case and vanishing temperature. The screened scattering potential is related to the static dielectric function and is written as $V(\boldsymbol{q}) = v_c(q)/\epsilon_{\rm RPA}(\boldsymbol{q})$. Here, the static dielectric function $\epsilon_{\rm RPA}(\boldsymbol{q}) = 1 - v_c(q)\Pi(\boldsymbol{q};0)$.

1. *Static polarizability function*

The static polarizability $\Pi(\boldsymbol{q};0)$ for $\varepsilon_{\rm F}$ to be in the conduction band of the surface of a TI is given by $\Pi(\boldsymbol{q};0) = \Pi^+(\boldsymbol{q};0) + \Pi^-(\boldsymbol{q};0)$, where

$$\Pi^+(\boldsymbol{q};0) = \sum_{\boldsymbol{k}}\Bigg[a_1(\boldsymbol{k},\boldsymbol{k}+\boldsymbol{q})\frac{n_{\rm F}(\varepsilon_{\boldsymbol{k}2}) - n_{\rm F}(\varepsilon_{\boldsymbol{k}+\boldsymbol{q}2})}{\varepsilon_{\boldsymbol{k}2} - \varepsilon_{\boldsymbol{k}+\boldsymbol{q}2}} + \bar{a}_1(\boldsymbol{k},\boldsymbol{k}+\boldsymbol{q})\frac{n_{\rm F}(\varepsilon_{\boldsymbol{k}2}) + n_{\rm F}(\varepsilon_{\boldsymbol{k}+\boldsymbol{q}2})}{\varepsilon_{\boldsymbol{k}2} + \varepsilon_{\boldsymbol{k}+\boldsymbol{q}2}}\Bigg], \tag{30}$$

$$\Pi^-(\boldsymbol{q};0) = \sum_{\boldsymbol{k}}\left[\bar{a}_1(\boldsymbol{k},\boldsymbol{k}+\boldsymbol{q})\frac{n_{\rm F}(\varepsilon_{\boldsymbol{k}1}) + n_{\rm F}(\varepsilon_{\boldsymbol{k}+\boldsymbol{q}1})}{\varepsilon_{\boldsymbol{k}1} + \varepsilon_{\boldsymbol{k}+\boldsymbol{q}1}}\right]. \tag{31}$$

Here, $\bar{a}_1(\boldsymbol{k},\boldsymbol{k}+\boldsymbol{q}) = 1 - a_1(\boldsymbol{k},\boldsymbol{k}+\boldsymbol{q})$. The long-wavelength Thomas-Fermi (TF) screening is important for charged-impurity scattering. In the $q \to 0$ limit, it is found that $a_1(\boldsymbol{k},\boldsymbol{k}+\boldsymbol{q}) \to 1$. Hence, $\Pi^-(q \to 0,\theta_{\boldsymbol{q}};0) \to 0$, and the polarizability $\Pi(q \to 0,\theta_{\boldsymbol{q}};0)$ is determined by the first term of Eq. (30). At zero temperature, we have

$$\Pi(q \to 0,\theta_{\boldsymbol{q}};0) = -\frac{\varepsilon_{\rm F}}{2\pi^2}\int_0^{2\pi}d\theta_{\boldsymbol{k}}\frac{\cos(\theta_{\boldsymbol{k}} - \theta_{\boldsymbol{q}})}{\Lambda(\theta_{\boldsymbol{k}},\theta_{\boldsymbol{q}})}, \tag{32}$$

where the angle-related function $\Lambda(\theta_{\boldsymbol{k}},\theta_{\boldsymbol{q}}) = 2v_{\rm F}^2\cos(\theta_{\boldsymbol{k}} - \theta_{\boldsymbol{q}}) + 3\lambda^2k_{\rm F}^4(\theta_{\boldsymbol{k}})[\cos(\theta_{\boldsymbol{k}} - \theta_{\boldsymbol{q}}) + \cos(5\theta_{\boldsymbol{k}} + \theta_{\boldsymbol{q}})]$. $k_{\rm F}(\theta_{\boldsymbol{k}})$ is the Fermi momentum relying on the azimuthal angle, determined by $\sqrt{v_{\rm F}^2k_{\rm F}^2(\theta_{\boldsymbol{k}}) + \lambda^2k_{\rm F}^6(\theta_{\boldsymbol{k}})(\cos 3\theta_{\boldsymbol{k}})^2} = \varepsilon_{\rm F}$. For weak λ, it has the form

$$k_{\rm F}(\theta_{\boldsymbol{k}}) = \frac{\varepsilon_{\rm F}}{v_{\rm F}} - \frac{1}{4}\frac{\lambda^2\varepsilon_{\rm F}^5}{v_{\rm F}^7}(1 + \cos 6\theta_{\boldsymbol{k}}). \tag{33}$$

In the $\lambda \to 0$ limit, the Fermi momentum tends to the previous result.[13] According to $N = 1/(8\pi^2)\int_0^{2\pi}d\theta_{\boldsymbol{k}}k_{\rm F}^2(\theta_{\boldsymbol{k}})$, the relation between the carrier density and Fermi energy is given by

$$N = \frac{1}{4\pi}\left[\left(\frac{\varepsilon_{\rm F}}{v_{\rm F}}\right)^2 - \frac{1}{2}\frac{\varepsilon_{\rm F}^6}{v_{\rm F}^8}\lambda^2\right]. \tag{34}$$

It should be noted that for our case, only the magnitude of momentum $\boldsymbol{q}$ tends to zero in the long-wavelength limit.

Therefore, the resultant polarizability $\Pi(q \to 0, \theta_{\boldsymbol{q}}; 0)$ may still rely on the azimuthal angle of $\boldsymbol{q}$, which is completely different from the two-dimensional Lindhard function[33] and the corresponding polarizability function of graphene.[34,35] For weak λ, the integral of Eq. (32) can be calculated analytically, and the TF dielectric function reduces to

$$\epsilon_{\rm TF}(\boldsymbol{q}) = 1 + \frac{k_{\rm TF}(\theta_{\boldsymbol{q}})}{q} \tag{35}$$

with the angle-dependent TF wave vector $k_{\rm TF}(\theta_{\boldsymbol{q}})$ where

$$k_{\rm TF}(\theta_{\boldsymbol{q}}) = \frac{e^2 \varepsilon_{\rm F}}{8\pi \epsilon_0 \kappa v_{\rm F}^8}\left[2v_{\rm F}^6 - 3\lambda^2 \varepsilon_{\rm F}^4 (1 + \cos 6\theta_{\boldsymbol{q}})\right]. \tag{36}$$

This dielectric function $\epsilon_{\rm TF}(\boldsymbol{q})$ tends to the previous result[13,35] when $\lambda \to 0$. We emphasize again that the angle dependence of the dielectric function originates from the cubic term in the Hamiltonian. The λ-related term becomes important when $v_{\rm F}^6 = \lambda^2 \varepsilon_{\rm F}^4$, corresponding to $\varepsilon_{\rm F} = 0.26$ eV in Bi_2Te_3, a density of 10^{13} cm^{-2}, which is a realistic density in the Bi_2Te_3 sample.[11]

2. Numerical results

It is seen that the polarizability function of Eq. (29) satisfies $\Pi(q, \theta_{\boldsymbol{q}}; \omega) = \Pi(q, \theta_{\boldsymbol{q}} - \pi; \omega) = \Pi(q, \theta_{\boldsymbol{q}} + \pi; \omega)$. Consequently, the angle relation of the scattering potential of Eq. (22) still holds for this screened Coulomb potential. Hence, when the carriers are scattered by the screened Coulomb form, only the longitudinal conductivity and y component of the CISP are nonzero. Now we numerically calculate the longitudinal conductivity and spin polarization for both TF screening and RPA screening. The following parameters in Bi_2Te_3 are used in the calculation:[13,25] Fermi velocity $v_{\rm F} = 2.55$ eV Å, warping parameter $\lambda = 250$ eV Å^3, impurity density $n_i = 10^{13}$ cm^{-2}, static dielectric constant $\kappa = 200$, and DC electric field $E = 10$ V/m. The results are plotted in Fig. 1. The corresponding conductivity and CISP for $\lambda = 0$ are also plotted for comparison. For vanishing λ, the conductivity and spin polarization linearly rely on the surface-carrier density N, which agrees with the previous theoretical calculation.[13] With increasing density N, the hexagonal-warping effect becomes important for both TF- and RPA-screened Coulomb potentials, leading to nonlinear characters of the conductivity and CISP. The magnitudes of the conductivity and spin polarization in the presence of the warping effect are larger than those in the absence of warping. Furthermore, we verify that $\sigma_{xx} = c_1 N + c_2 N^2$ and $S_y = c_3 N + c_4 N^2$ in contrast to short-range scattering. We note that the TF screening is the long-wavelength limit of the RPA dielectric function. At the same time, for a finite magnitude of momentum, the RPA screening is weaker than that of the TF. Hence, the conductivity of the TF-screened Coulomb potential is larger than that of the RPA at the same λ.

Here, we have assumed that the impurities are located right on the surface. However, the charged impurities in the bulk of TIs may also contribute to the surface transport. These remote impurities will enhance the magnitude of the conductivity and spin polarization. One can deduce that the warping will lead to a large increase of the magnitude of the surface-transport quantities even in the presence of remote impurities.

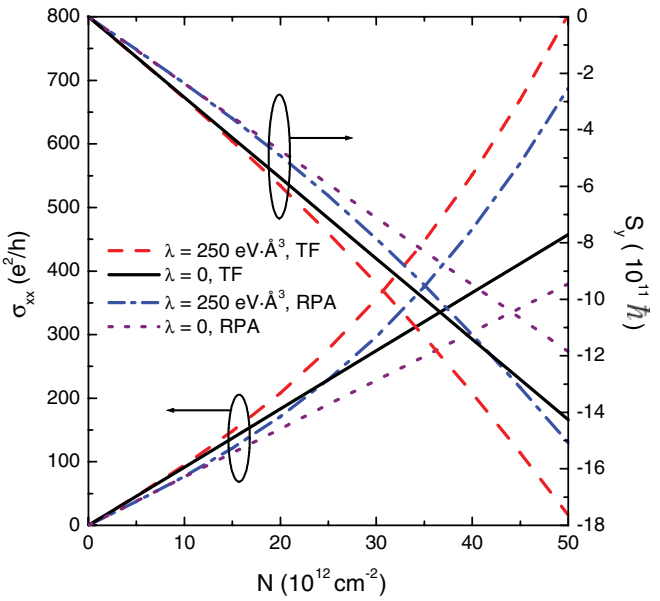

FIG. 1. (Color online) The longitudinal conductivity and CISP scattered by screened charged impurities as functions of the surface-carrier density for both TF screening and RPA screening.

Note that the classical surface conductivity of Bi_2Se_3 was observed by using a gate electrode.[14] It showed a linear carrier-density dependence when the density was smaller than the carrier density above which the bulk conduction band is populated. In Bi_2Se_3, the hexagonal warping is small enough to be omitted completely. Hence, this experiment verified the previous theoretical prediction well.[13] However, for the surface states of TIs for which the warping term cannot be neglected such as Bi_2Te_3, the linear dependence will be broken, and a quadratic relation also appears. Therefore, our prediction suggests that the surface transport in Bi_2Te_3 should be different from that of Bi_2Se_3, and one should be very careful when one analyzes the surface-transport data of Bi_2Te_3.

IV. CLASSICAL TRANSPORT IN THE PRESENCE OF MAGNETIC SCATTERING

Let us now address the magnetic-scattering case in the classical diffusion regime for which the scattering potential reads[36]

$$\widetilde{V}(\boldsymbol{r}) = \sum_{\{\boldsymbol{R}_\alpha\}} \{J_\parallel [s_x(\boldsymbol{r})\tilde{S}_x(\boldsymbol{R}_\alpha) + s_y(\boldsymbol{r})\tilde{S}_y(\boldsymbol{R}_\alpha)] + J_z s_z(\boldsymbol{r})\tilde{S}_z(\boldsymbol{R}_\alpha)\}\delta(\boldsymbol{r} - \boldsymbol{R}_\alpha). \tag{37}$$

Here, $\boldsymbol{s} = \frac{1}{2}\boldsymbol{\sigma}$ is the spin vector of the electron, $\tilde{\boldsymbol{S}}$ is the impurity spin, and $J_\parallel$ and J_z are the coupling parameters.

For simplicity, we assume classical magnetic impurities and their spins, which are polarized in the z direction. This kind of potential conserves the z component of the carrier spin. It is known that magnetic doping will open a gap in the helical Dirac cone.[37] From the mean-field approximation, the gap has the form[15] $\Delta = 2n_i J_z \tilde{S}$. Hence, for a high-mobility sample, the density of magnetic impurities is small enough, and then the gap opened by the magnetic doping is considered to be very small. When $\Delta \ll \varepsilon_{\rm F}$, the effect of the gap on

the energy spectrum, group velocity, etc. can be neglected safely. Therefore, we can only consider the scattering effect of magnetic impurities. Applying a similar procedure as that used for the nonmagnetic-scattering situation, the analogous kinetic equations can be derived only by replacing $V(\boldsymbol{k}-\boldsymbol{q})$, $a_1(\boldsymbol{k},\boldsymbol{q})$, $a_2(\boldsymbol{k},\boldsymbol{q})$, and $a_3(\boldsymbol{k},\boldsymbol{q})$ in Eqs. (9)–(11) with $u_{\rm M}$, $a_1^{\rm M}(\boldsymbol{k},\boldsymbol{q})$, $a_2^{\rm M}(\boldsymbol{k},\boldsymbol{q})$, and $a_3^{\rm M}(\boldsymbol{k},\boldsymbol{q})$, respectively. Here, $u_{\rm M}=J_z\tilde{S}/2$ and

$$a_1^{\rm M}(\boldsymbol{k},\boldsymbol{q}) = -\tfrac{1}{2}[\sin 2\beta_{\boldsymbol{k}}\sin 2\beta_{\boldsymbol{q}}\cos(\theta_{\boldsymbol{k}}-\theta_{\boldsymbol{q}}) - \cos 2\beta_{\boldsymbol{k}}\cos 2\beta_{\boldsymbol{q}} - 1], \quad (38)$$

$$a_2^{\rm M}(\boldsymbol{k},\boldsymbol{q}) = -\tfrac{1}{2}[\cos 2\beta_{\boldsymbol{k}}\sin 2\beta_{\boldsymbol{q}}\cos(\theta_{\boldsymbol{k}}-\theta_{\boldsymbol{q}}) + \sin 2\beta_{\boldsymbol{k}}\cos 2\beta_{\boldsymbol{q}}], \quad (39)$$

$$a_3^{\rm M}(\boldsymbol{k},\boldsymbol{q}) = \tfrac{1}{2}\sin 2\beta_{\boldsymbol{q}}\sin(\theta_{\boldsymbol{k}}-\theta_{\boldsymbol{q}}). \quad (40)$$

Taking into account the symmetrical property of the distribution function, it is also verified that only the longitudinal conductivity and y component of the CISP are nonzero for this magnetic scattering. Eventually, their expressions are given by Eqs. (23) and (24).

We first assume that the warping parameter is weak. Thus the kinetic equation can be solved analytically, and the diagonal element of the impurity-related distribution is

$$\rho_{22}^{(2)}(\boldsymbol{k}) = -\frac{2eE}{3n_i u_{\rm M}^2}\left[\frac{2v_{\rm F}^3}{\varepsilon_{\rm F}}\cos\theta_{\boldsymbol{k}} + \lambda^2\frac{\varepsilon_{\rm F}^3}{2v_{\rm F}^3}\left(\frac{35}{3}\cos\theta_{\boldsymbol{k}} + \frac{17}{2}\cos 5\theta_{\boldsymbol{k}} - \frac{1}{2}\cos 7\theta_{\boldsymbol{k}}\right)\right]\delta(\varepsilon_{k2}-\varepsilon_{\rm F}). \quad (41)$$

Hence, the charge conductivity and CISP are written as

$$\sigma_{xx} = \frac{e^2}{9\pi n_i u_{\rm M}^2}\left[3v_{\rm F}^2 + 8\left(\frac{\varepsilon_{\rm F}}{v_{\rm F}}\right)^4\lambda^2\right] = \frac{e^2}{9\pi n_i u_{\rm M}^2}\left(3v_{\rm F}^2 + 128\pi^2\lambda^2N^2\right), \quad (42)$$

$$S_y = -\frac{eE}{36\pi n_i u_{\rm M}^2}\left(6v_{\rm F} + 7\frac{\varepsilon_{\rm F}^4}{v_{\rm F}^5}\lambda^2\right) = -\frac{eE}{18\pi v_{\rm F} n_i u_{\rm M}^2}\left(3v_{\rm F}^2 + 56\pi^2\lambda^2N^2\right). \quad (43)$$

Compared with the short-range nonmagnetic scattering, similar density-dependent behaviors have also been seen for this magnetic one. However, the concrete coefficients are completely distinct.

To go beyond the weak warping case, we now numerically solve the kinetic equations. Setting the relaxation time $\tau = 2v_{\rm F}/(n_i u_{\rm M}^2\sqrt{4\pi N_0}) = 1$ ps with $N_0 = 10^{12}$ cm^{-2}, the obtained longitudinal conductivity and spin polarization are plotted in Fig. 2. For comparison, the conductivity and CISP without the warping effect are also calculated. It is seen that for a fixed relaxation time, the warping term also has an important role in the surface transport of a three-dimensional TI. The magnitudes of the longitudinal conductivity and spin polarization increase drastically with increasing surface density. Note that the above analytical results of Eqs. (42) and (43) are valid for weak warping, that is, a density $N \ll v_{\rm F}/(5\pi\lambda) \approx 5\times10^{12}$ cm^{-2}. For example, if we use the approximation result of Eq. (42)

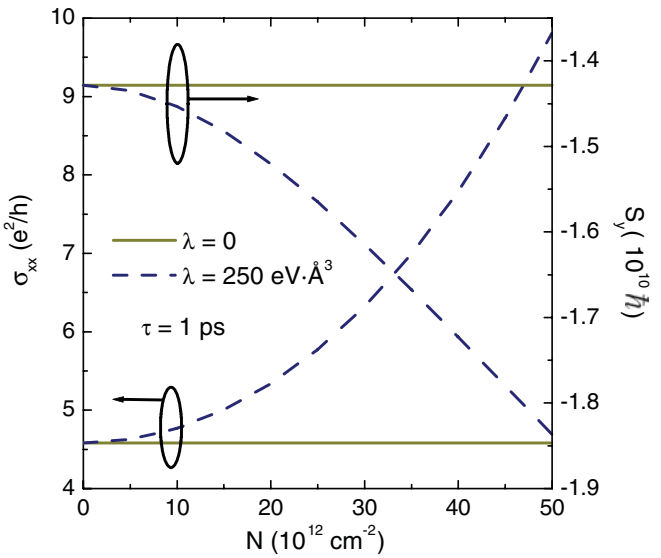

FIG. 2. (Color online) The longitudinal conductivity and y component of the CISP scattered by magnetic impurities as a function of the surface-carrier density. The other parameters are the same as those in Sec. III D 2.

to estimate the conductivity, the resultant $\sigma_{xx} \approx 171.3$ e^2/h when $N = 30\times10^{12}$ cm^{-2}. This value is much larger than the numerical one. At the same time, it can be confirmed from the numerical calculation that the additional terms $\propto N$ also contribute to the conductivity and spin polarization for nonvanishing warping.

V. QUANTUM CORRECTION

We now focus on the effect of weak warping on the quantum corrections to the conductivity and spin polarization. For this surface state, the Berry phase is calculated as

$$\gamma = -i\int_0^{2\pi} d\theta_{\boldsymbol{k}}\langle\varphi_{k2}|\frac{\partial}{\partial\theta_{\boldsymbol{k}}}|\varphi_{k2}\rangle = \frac{1}{2}\int_0^{2\pi} d\theta_{\boldsymbol{k}}\left[1 + \frac{\lambda k_{\rm F}^3(\theta_{\boldsymbol{k}})}{\varepsilon_{\rm F}}\cos 3\theta_{\boldsymbol{k}}\right]. \quad (44)$$

In connection with Eq. (33), the Berry phase equals π. Hence, weak antilocalization is expected for the surface state even in the presence of the warping effect.

Using the equilibrium Green's function, the quantum corrections are described by the diagrams in Fig. 3. Firstly, we consider the short-range nonmagnetic scattering. Note that in the previous work, the authors replaced the energy spectrum with its angle-average one to investigate the quantum correction. In our situation the angle dependence of the warping is taken into account; hence, our treatment is beyond this approximation. We also assume that the Fermi energy is in the gap of the bulk band and crosses the upper band of the surface state. Under the Born approximation, the impurity-averaged-equilibrium retarded and advanced Green's functions are given by

$$\hat{G}_{\boldsymbol{k}}^{r/a}(\epsilon) = \frac{1}{\epsilon - \epsilon_{\boldsymbol{k}} \pm i/2\tau_e} \quad (45)$$

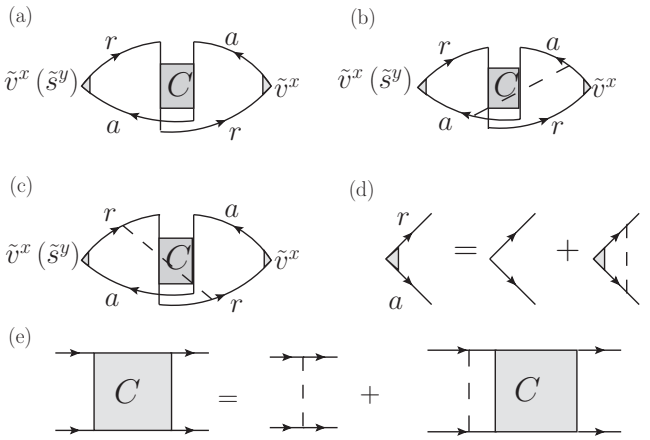

FIG. 3. Diagrams for the quantum corrections to the surface conductivity and spin polarization of a TI. (a) Bare and (b) and (c) two dressed Hikami boxes. (d) Equation for the vertex correction to the velocity and the average spin in the ladder approximation. (e) Bethe-Salpeter equation for the Cooperon. The arrowed-solid and dashed lines represent the retarded and advanced Green's functions and scattering potential, respectively.

with the relaxation time $1/\tau_e = n_i u^2[\varepsilon_F/(4v_F^8)](2v_F^6 - 3\varepsilon_F^4\lambda^2)$. We add hats to the equilibrium Green's functions to distinguish them from the nonequilibrium Green's functions. Notice that we have used a matrix distribution function to discuss the classical transport. However, in the absence of an interband-transition process and for usual elastic scattering, the matrix distribution reduces to a scalar one [see Eqs. (9), (23), and (24)]. Hence, the kinetic-equation approach is in principle equivalent to that of the one-band equilibrium Green's functions. The kinetic-equation approach can easily deal with momentum-dependent scattering in classical transport, but it is difficult to discuss the quantum correction. Therefore, we treat the weak antilocalization in the diagrammatic approach by using equilibrium Green's functions. Below, the word *equilibrium* will be omitted for brevity.

In the calculation, the vertex corrections to the bare velocity and average spin [Fig. 3(d)] should be taken into account, and they are written as

$$\tilde{v}_{\boldsymbol{k}}^x = 2v_F\cos\theta_{\boldsymbol{k}} + \frac{\lambda^2 k^4}{2v_F}\left(3\cos\theta_{\boldsymbol{k}} + \frac{5}{2}\cos 5\theta_{\boldsymbol{k}} - \frac{1}{2}\cos 7\theta_{\boldsymbol{k}}\right), \tag{46}$$

$$\tilde{s}_{\boldsymbol{k}}^y = \cos\theta_{\boldsymbol{k}} - \frac{\lambda^2 k^4}{4v_F^2}\left(3\cos\theta_{\boldsymbol{k}} + \frac{1}{2}\cos 5\theta_{\boldsymbol{k}} + \frac{1}{2}\cos 7\theta_{\boldsymbol{k}}\right). \tag{47}$$

Different from the topological surface states in the absence of hexagonal warping, the velocity and spin vertices become anisotropic. This anisotropy is very important and will lead to the density dependence of the quantum correction. Note that in the absence of warping, the group velocity $v_{\boldsymbol{k}}^x = \partial\epsilon_{\boldsymbol{k}}/\partial k_x|_{\lambda=0} = v_F\cos\theta_{\boldsymbol{k}}$ and average spin $s_{\boldsymbol{k}}^y = \frac{1}{2}\langle\varphi_{\boldsymbol{k}2}|\hat{\sigma}_y|\varphi_{\boldsymbol{k}2}\rangle|_{\lambda=0} = \frac{1}{2}\cos\theta_{\boldsymbol{k}}$. Therefore, for vanishing λ, the velocity vertex reduces to $\tilde{v}_{\boldsymbol{k}}^x = 2v_{\boldsymbol{k}}^x$.[23]

In addition to the bare Hikami box of Fig. 3(a), two dressed Hikami boxes [Figs. 3(b) and 3(c)] are also needed in the calculation of quantum corrections, and the total correction of the charge conductivity is given by

$$\delta\sigma_{xx} = \delta\sigma_{xx}^{(1)} + \delta\sigma_{xx}^{(2)} + \delta\sigma_{xx}^{(3)}, \tag{48}$$

where the quantum correction due to a bare Hikami box is

$$\delta\sigma_{xx}^{(1)} = \frac{e^2}{2\pi}\sum_{\boldsymbol{k},\boldsymbol{q}} \tilde{v}_{\boldsymbol{k}}^x \hat{G}_{\boldsymbol{k}}^r \hat{G}_{\boldsymbol{q}-\boldsymbol{k}}^r \tilde{v}_{\boldsymbol{q}-\boldsymbol{k}}^x \hat{G}_{\boldsymbol{q}-\boldsymbol{k}}^a \hat{G}_{\boldsymbol{k}}^a C(\boldsymbol{q}), \tag{49}$$

and the quantum corrections due to two dressed Hikami boxes are

$$\delta\sigma_{xx}^{(2)} = \frac{e^2}{2\pi}\sum_{\boldsymbol{k},\boldsymbol{q},\boldsymbol{k}'} \tilde{v}_{\boldsymbol{k}}^x \hat{G}_{\boldsymbol{k}}^r \hat{G}_{\boldsymbol{k}'}^r \langle|\xi_{\boldsymbol{k}\boldsymbol{k}'}|^2\rangle_{\rm imp} \hat{G}_{\boldsymbol{q}-\boldsymbol{k}}^r \hat{G}_{\boldsymbol{q}-\boldsymbol{k}'}^r \times \tilde{v}_{\boldsymbol{q}-\boldsymbol{k}'}^x \hat{G}_{\boldsymbol{q}-\boldsymbol{k}'}^a \hat{G}_{\boldsymbol{k}}^a C(\boldsymbol{q}), \tag{50}$$

$$\delta\sigma_{xx}^{(3)} = \frac{e^2}{2\pi}\sum_{\boldsymbol{k},\boldsymbol{q},\boldsymbol{k}'} \tilde{v}_{\boldsymbol{k}}^x \hat{G}_{\boldsymbol{k}}^r \hat{G}_{\boldsymbol{q}-\boldsymbol{k}'}^r \langle|\xi_{\boldsymbol{k}\boldsymbol{k}'}|^2\rangle_{\rm imp} \hat{G}_{\boldsymbol{q}-\boldsymbol{k}'}^a \hat{G}_{\boldsymbol{q}-\boldsymbol{k}}^a \times \tilde{v}_{\boldsymbol{q}-\boldsymbol{k}'}^x \hat{G}_{\boldsymbol{k}'}^a \hat{G}_{\boldsymbol{k}}^a C(\boldsymbol{q}). \tag{51}$$

Here, $\xi_{\boldsymbol{k}\boldsymbol{k}'} = \int d\boldsymbol{r} e^{i(\boldsymbol{k}'-\boldsymbol{k})\cdot\boldsymbol{r}}\langle\varphi_{\boldsymbol{k}2}|\widetilde{V}(\boldsymbol{r})|\varphi_{\boldsymbol{k}'2}\rangle$ is the scattering amplitude between two eigenstates. $\langle\cdots\rangle_{\rm imp}$ indicates the average over all possible configurations of random impurities. Consequently, for δ-form impurity scattering, $\langle|\xi_{\boldsymbol{k}\boldsymbol{k}'}|^2\rangle_{\rm imp} = n_i u^2\langle\varphi_{\boldsymbol{k}2}|\varphi_{\boldsymbol{k}'2}\rangle\langle\varphi_{\boldsymbol{k}'2}|\varphi_{\boldsymbol{k}2}\rangle$. Since the Cooperon $C(\boldsymbol{q})$ diverges as $q \to 0$, the most divergent terms can be obtained by setting $\boldsymbol{q} = 0$ for the velocity vertex and the retarded and advanced Green's functions in the above expressions. Calculating momentum $\boldsymbol{k}$ and $\boldsymbol{k}'$ integrals, the total conductivity correction is written as

$$\delta\sigma_{xx} = -\frac{e^2}{\pi}\varepsilon_F\tau_e^3\left(1 + \frac{\lambda^2\varepsilon_F^4}{2v_F^6}\right)\sum_{\boldsymbol{q}} C(\boldsymbol{q}). \tag{52}$$

For vanishing λ, this result is in accordance with that of Ref. 21. Similarly, the total spin-polarization correction is given by

$$\delta S_y = \frac{eE}{2\pi}\frac{\varepsilon_F\tau_e^3}{v_F}\left(1 - \frac{\lambda^2\varepsilon_F^4}{v_F^6}\right)\sum_{\boldsymbol{q}} C(\boldsymbol{q}). \tag{53}$$

The Cooperon satisfies the Bethe-Salpeter equation [Fig. 3(e)]:

$$C_{\boldsymbol{k}_1\boldsymbol{k}_2} = C_{\boldsymbol{k}_1\boldsymbol{k}_2}^{(0)} + \sum_{\boldsymbol{k}'} C_{\boldsymbol{k}_1\boldsymbol{k}'}^{(0)} G_{\boldsymbol{k}'}^r G_{\boldsymbol{q}-\boldsymbol{k}'}^a C_{\boldsymbol{k}'\boldsymbol{k}_2} = C_{\boldsymbol{k}_1\boldsymbol{k}_2}^{(0)} + \int \frac{dk'd\theta_{\boldsymbol{k}'}}{(2\pi)^2} F(\boldsymbol{k}_1,\boldsymbol{k}',\boldsymbol{q}) C_{\boldsymbol{k}'\boldsymbol{k}_2}, \tag{54}$$

where $\boldsymbol{k}_1 + \boldsymbol{k}_2 = \boldsymbol{q}$ and $F(\boldsymbol{k}_1,\boldsymbol{k}',\boldsymbol{q}) = k' C_{\boldsymbol{k}_1\boldsymbol{k}'}^{(0)} \hat{G}_{\boldsymbol{k}'}^r \hat{G}_{\boldsymbol{q}-\boldsymbol{k}'}^a$, and by expanding up to λ^2, the bare vertex $C_{\boldsymbol{k}_1\boldsymbol{k}_2}^{(0)}$ for small q is

written as

$$C^{(0)}_{\boldsymbol{k}_1\boldsymbol{k}_2} = \Upsilon^{(0)}_{\boldsymbol{k}_1\boldsymbol{k}_2} + \lambda^2\Upsilon^{(2)}_{\boldsymbol{k}_1\boldsymbol{k}_2} \tag{55}$$

with

$$\Upsilon^{(0)}_{\boldsymbol{k}_1\boldsymbol{k}_2} = \frac{v_{\mathrm{F}}^2}{2\varepsilon_{\mathrm{F}}\tau_e}[1 + 2e^{i(\theta_{\boldsymbol{k}_1}-\theta_{\boldsymbol{k}_2})} + e^{2i(\theta_{\boldsymbol{k}_1}-\theta_{\boldsymbol{k}_2})}]. \tag{56}$$

The expression of $\Upsilon^{(2)}_{\boldsymbol{k}_1\boldsymbol{k}_2}$ is long, and we do not present it here. For weak warping, the solution of Eq. (54) is found as $C_{\boldsymbol{k}_1\boldsymbol{k}_2} = \Lambda^{(0)}_{\boldsymbol{k}_1\boldsymbol{k}_2} + \lambda^2\Lambda^{(2)}_{\boldsymbol{k}_1\boldsymbol{k}_2}$. $\Lambda^{(0)}_{\boldsymbol{k}_1\boldsymbol{k}_2}$ and $\Lambda^{(2)}_{\boldsymbol{k}_1\boldsymbol{k}_2}$ are independent of λ. With the help of the expansion $F(\boldsymbol{k}_1,\boldsymbol{k}',\boldsymbol{q}) = F^{(0)}(\boldsymbol{k}_1,\boldsymbol{k}',\boldsymbol{q}) + \lambda^2 F^{(2)}(\boldsymbol{k}_1,\boldsymbol{k}',\boldsymbol{q})$, $\Lambda^{(0)}_{\boldsymbol{k}_1\boldsymbol{k}_2}$ and $\Lambda^{(2)}_{\boldsymbol{k}_1\boldsymbol{k}_2}$ are determined from the following equations:

$$\Lambda^{(0)}_{\boldsymbol{k}_1\boldsymbol{k}_2} = \Upsilon^{(0)}_{\boldsymbol{k}_1\boldsymbol{k}_2} + \int \frac{dk'd\theta_{\boldsymbol{k}'}}{(2\pi)^2} F^{(0)}(\boldsymbol{k}_1,\boldsymbol{k}',\boldsymbol{q})\Lambda^{(0)}_{\boldsymbol{k}_1\boldsymbol{k}_2}, \tag{57}$$

$$\Lambda^{(2)}_{\boldsymbol{k}_1\boldsymbol{k}_2} = \Upsilon^{(2)}_{\boldsymbol{k}_1\boldsymbol{k}_2} + \int \frac{dk'd\theta_{\boldsymbol{k}'}}{(2\pi)^2} F^{(2)}(\boldsymbol{k}_1,\boldsymbol{k}',\boldsymbol{q})\Lambda^{(0)}_{\boldsymbol{k}'\boldsymbol{k}_2} + \int \frac{dk'd\theta_{\boldsymbol{k}'}}{(2\pi)^2} F^{(0)}(\boldsymbol{k}_1,\boldsymbol{k}',\boldsymbol{q})\Lambda^{(2)}_{\boldsymbol{k}'\boldsymbol{k}_2}. \tag{58}$$

$\Lambda^{(0)}_{\boldsymbol{k}_1\boldsymbol{k}_2}$ can be acquired from Eq. (57), and then we can obtain $\Lambda^{(2)}_{\boldsymbol{k}_1\boldsymbol{k}_2}$ from Eq. (58). It is found that $F^{(0)}(\boldsymbol{k}_1,\boldsymbol{k}',\boldsymbol{q})$ relies on $\theta_{\boldsymbol{k}_1}$ through $\cos\theta_{\boldsymbol{k}_1}$, $\sin\theta_{\boldsymbol{k}_1}$, $\cos 2\theta_{\boldsymbol{k}_1}$, and $\sin 2\theta_{\boldsymbol{k}_1}$. Hence, $\Lambda^{(0)}_{\boldsymbol{k}_1\boldsymbol{k}_2}$ and $\Lambda^{(2)}_{\boldsymbol{k}_1\boldsymbol{k}_2}$ have the forms

$$\Lambda^{(0)}_{\boldsymbol{k}_1\boldsymbol{k}_2} = \Upsilon^{(0)}_{\boldsymbol{k}_1\boldsymbol{k}_2} + \mathcal{A}_0 + \mathcal{A}_1\cos\theta_{\boldsymbol{k}_1} + \mathcal{B}_1\sin\theta_{\boldsymbol{k}_1} + \mathcal{A}_2\cos 2\theta_{\boldsymbol{k}_1} + \mathcal{B}_2\sin 2\theta_{\boldsymbol{k}_1}, \tag{59}$$

$$\Lambda^{(2)}_{\boldsymbol{k}_1\boldsymbol{k}_2} = \Upsilon^{(2)}_{\boldsymbol{k}_1\boldsymbol{k}_2} + \int \frac{dk'd\theta_{\boldsymbol{k}'}}{(2\pi)^2} F^{(2)}(\boldsymbol{k}_1,\boldsymbol{k}',\boldsymbol{q})\Lambda^{(0)}_{\boldsymbol{k}'\boldsymbol{k}_2} + \mathcal{C}_0 + \mathcal{C}_1\cos\theta_{\boldsymbol{k}_1} + \mathcal{D}_1\sin\theta_{\boldsymbol{k}_1} + \mathcal{C}_2\cos 2\theta_{\boldsymbol{k}_1} + \mathcal{D}_2\sin 2\theta_{\boldsymbol{k}_1}. \tag{60}$$

The above coefficients $\mathcal{A}_i$, $\mathcal{B}_j$, $\mathcal{C}_i$, and $\mathcal{D}_j$ ($i = 0,1,2$ and $j = 1,2$) are independent of $\theta_{\boldsymbol{k}_1}$ and can be determined by Eqs. (57) and (58). The derivations are tedious but direct. By setting $\boldsymbol{k}_1 = \boldsymbol{k}$, $\boldsymbol{k}_2 = \boldsymbol{q} - \boldsymbol{k}$ and $\theta_{\boldsymbol{k}_1} - \theta_{\boldsymbol{k}_2} = \pi$ for small q, and collecting the most divergent terms, the Cooperon is finally obtained as

$$C(\boldsymbol{q}) = -\frac{1}{\varepsilon_{\mathrm{F}}\tau_e^3 q^2} - \frac{5}{4}\frac{\lambda^2\varepsilon_{\mathrm{F}}^3}{v_{\mathrm{F}}^6\tau_e^3 q^2}. \tag{61}$$

By performing the integration over q between $1/l_\phi$ and $1/l$, the logarithmic corrections to the conductivity and spin polarization are found as

$$\delta\sigma_{xx} = \frac{e^2}{4\pi^2}\left(1 + \frac{3}{4}\frac{\lambda^2\varepsilon_{\mathrm{F}}^4}{v_{\mathrm{F}}^6}\right)\ln\frac{\tau_\phi}{\tau_e}, \tag{62}$$

$$\delta S_y = -\frac{eE}{8\pi^2 v_{\mathrm{F}}}\left(1 + \frac{1}{4}\frac{\lambda^2\varepsilon_{\mathrm{F}}^4}{v_{\mathrm{F}}^6}\right)\ln\frac{\tau_\phi}{\tau_e}. \tag{63}$$

Here, we use the relations $l = \sqrt{D\tau_e}$ and $l_\phi = \sqrt{D\tau_\phi}$, where D is the diffusion constant. It is useful to rewrite the conductivity correction as $\delta\sigma_{xx} = -\alpha[e^2/(2\pi^2)]\ln(\tau_\phi/\tau_e)$. Therefore, α has the form

$$\alpha = -\frac{1}{2}\left(1 + \frac{3}{4}\frac{\lambda^2\varepsilon_{\mathrm{F}}^4}{v_{\mathrm{F}}^6}\right) = -\frac{1}{2}\left(1 + \frac{12\pi^2\lambda^2}{v_{\mathrm{F}}^2}N^2\right). \tag{64}$$

The hexagonal warping makes the prefactor α quadratically depend on the carrier density, and it is always smaller than $-1/2$ in vivid contrast with the angle-average approximation.[22] For vanishing warping, this factor becomes $-1/2$ in agreement with the theoretical work.[21] We note that the above formula is fulfilled for weak warping. On the other hand, one can estimate the α for Bi_2Te_3 at the low surface density $N \ll 10^{13}$ cm^{-2}. For instance, $\alpha \approx -0.506$ when $N = 10^{12}$ cm^{-2}. However, the value of the α obtained from a fit in a recent experiment[19] was -0.39, which is larger than -0.5, conflicting with our formula. This may be due to the inevitable bulk-state contribution in three-dimensional TIs.[38] The experimental observation of α is a collective result of the surface bands and bulk bands. The bulk channels may result in a weak localization term, which could reduce or even compensate the weak antilocalization arising from the surface states. Therefore, a larger value of α is obtained experimentally. In contrast to the surface band, the bulk sub-band of a TI has a quadratic term and large band gap. As a result, a different density-dependent behavior of the quantum correction is expected for the bulk channels. A quantitative measurement of the carrier-density-dependent surface-conductivity correction could be helpful for distinguishing the surface contribution from the bulk one.

In the presence of magnetic scattering, the divergence of $C(\boldsymbol{q})$ when $q \to 0$ vanishes, which is analogous to the case without warping.[21] Therefore, the logarithmic correction disappears, and it can be deduced that the magnetic scattering suppresses the weak antilocalization effect in the presence of both magnetic and nonmagnetic scattering. This is in accordance with experimental observation.[19]

VI. CONCLUSION

In summary, we have investigated the surface transport of a three-dimensional TI in both the classical and quantum diffusive regimes. In this study, we include the role of the hexagonal-warping correction of the Fermi surface. It is found that the hexagonal warping has drastic effects on the surface conductivity and CISP of a three-dimensional TI for both nonmagnetic and magnetic elastic scattering. For a surface state with large warping, such as that of Bi_2Te_3, an additional quadratic carrier-density dependence is found in both regimes. Because the carrier density can be controlled by the gate voltage, we hope that our predictions will soon be verified experimentally.

ACKNOWLEDGMENTS

This work was supported by the National Science Foundation of China (Grant Nos. 11104002 and 60876064).

*cmwangsjtu@gmail.com

[1] C. L. Kane and E. J. Mele, Phys. Rev. Lett. **95**, 226801 (2005).
[2] X.-L. Qi, T. L. Hughes, and S.-C. Zhang, Phys. Rev. B **78**, 195424 (2008).
[3] X. L. Qi and S. C. Zhang, e-print arXiv:1008.2026 (unpublished).
[4] L. Fu and C. L. Kane, Phys. Rev. Lett. **100**, 096407 (2008).
[5] I. Garate and M. Franz, Phys. Rev. Lett. **104**, 146802 (2010).
[6] C. Wu, B. A. Bernevig, and S.-C. Zhang, Phys. Rev. Lett. **96**, 106401 (2006).
[7] C. Xu and J. E. Moore, Phys. Rev. B **73**, 045322 (2006).
[8] K. S. Novoselov, A. K. Geim, S. V. Morozov, D. Jiang, M. I. Katsnelson, I. V. Grigorieva, S. V. Dubonos, and A. A. Firsov, Nature (London) **438**, 197 (2005).
[9] D. Hsieh, D. Qian, L. Wray, Y. Xia, Y. S. Hor, R. J. Cava, and M. Z. Hasan, Nature (London) **452**, 970 (2008).
[10] D. Hsieh, Y. Xia, L. Wray, D. Qian, A. Pal, J. H. Dil, J. Osterwalder, F. Meier, G. Bihlmayer, C. L. Kane, Y. S. Hor, R. J. Cava, and M. Z. Hasan, Science **323**, 919 (2009).
[11] Y. L. Chen, J. G. Analytis, J.-H. Chu, Z. K. Liu, S.-K. Mo, X. L. Qi, H. J. Zhang, D. H. Lu, X. Dai, Z. Fang, S. C. Zhang, I. R. Fisher, Z. Hussain, and Z.-X. Shen, Science **325**, 178 (2009).
[12] J. G. Checkelsky, Y. S. Hor, R. J. Cava, and N. P. Ong, Phys. Rev. Lett. **106**, 196801 (2011).
[13] D. Culcer, E. H. Hwang, T. D. Stanescu, and S. Das Sarma, Phys. Rev. B **82**, 155457 (2010).
[14] D. Kim, S. Cho, N. P. Butch, P. Syers, K. Kirshenbaum, J. Paglione, and M. S. Fuhrer, e-print arXiv:1105.1410 (unpublished).
[15] D. Culcer and S. Das Sarma, Phys. Rev. B **83**, 245441 (2011).
[16] S. Giraud and R. Egger, Phys. Rev. B **83**, 245322 (2011).
[17] T. Yokoyama and S. Murakami, Phys. Rev. B **83**, 161407(R) (2011).
[18] J. Chen, H. J. Qin, F. Yang, J. Liu, T. Guan, F. M. Qu, G. H. Zhang, J. R. Shi, X. C. Xie, C. L. Yang, K. H. Wu, Y. Q. Li, and L. Lu, Phys. Rev. Lett. **105**, 176602 (2010).
[19] H.-T. He, G. Wang, T. Zhang, I.-K. Sou, G. K. L. Wong, J.-N. Wang, H.-Z. Lu, S.-Q. Shen, and F.-C. Zhang, Phys. Rev. Lett. **106**, 166805 (2011).
[20] M. Liu, C.-Z. Chang, Z. Zhang, Y. Zhang, W. Ruan, K. He, L.-L. Wang, X. Chen, J.-F. Jia, S.-C. Zhang, Q.-K. Xue, X. Ma, and Y. Wang, Phys. Rev. B **83**, 165440 (2011).
[21] H. Z. Lu, J. Shi, and S. Q. Shen, Phys. Rev. Lett. **107**, 076801 (2011).
[22] G. Tkachov and E. M. Hankiewicz, Phys. Rev. B **84**, 035444 (2011).
[23] E. McCann, K. Kechedzhi, V. I. Fal'ko, H. Suzuura, T. Ando, and B. L. Altshuler, Phys. Rev. Lett. **97**, 146805 (2006).
[24] Z. Alpichshev, J. G. Analytis, J.-H. Chu, I. R. Fisher, Y. L. Chen, Z. X. Shen, A. Fang, and A. Kapitulnik, Phys. Rev. Lett. **104**, 016401 (2010).
[25] L. Fu, Phys. Rev. Lett. **103**, 266801 (2009).
[26] H. Haug and A.-P. Jauho, *Quantum Kinetics in Transport and Optics of Semiconductors* (Springer, Berlin, 1996).
[27] M. I. D'yakonov and V. I. Perel', Phys. Lett. A **35**, 459 (1971).
[28] V. M. Edelstein, Solid State Commun. **73**, 233 (1990).
[29] C. M. Wang, S. Y. Liu, Q. Lin, X. L. Lei, and M. Q. Pang, J. Phys. Condens. Matter **22**, 095803 (2010).
[30] C. M. Wang, M. Q. Pang, S. Y. Liu, and X. L. Lei, Phys. Lett. A **374**, 1286 (2010).
[31] Y. Tokura, Phys. Rev. B **58**, 7151 (1998).
[32] Y. K. Kato, R. C. Myers, A. C. Gossard, and D. D. Awschalom, Science **306**, 1910 (2004).
[33] F. Stern, Phys. Rev. Lett. **18**, 546 (1967).
[34] B. Wunsch, T. Stauber, F. Sols, and F. Guinea, New J. Phys. **8**, 318 (2006).
[35] E. H. Hwang and S. Das Sarma, Phys. Rev. B **75**, 205418 (2007).
[36] Q. Liu, C.-X. Liu, C. Xu, X.-L. Qi, and S.-C. Zhang, Phys. Rev. Lett. **102**, 156603 (2009).
[37] Y. L. Chen, J.-H. Chu, J. G. Analytis, Z. K. Liu, K. Igarashi, H.-H. Kuo, X. L. Qi, S. K. Mo, R. G. Moore, D. H. Lu, M. Hashimoto, T. Sasagawa, S. C. Zhang, I. R. Fisher, Z. Hussain, and Z. X. Shen, Science **329**, 659 (2010).
[38] H. Z. Lu and S.-Q. Shen, Phys. Rev. B **84**, 125138 (2011).